Science
AAAS

A Cell Cycle Phosphoproteome of the Yeast Centrosome

Jamie M. Keck, *et al.*

Science **332**, 1557 (2011);
DOI: 10.1126/science.1205193

Science (print ISSN 0036-8075; online ISSN 1095-9203) is published weekly, except the last week in December, by the American Association for the Advancement of Science, 1200 New York Avenue NW, Washington, DC 20005.

it causes cells to become more resistant to the micromanipulations involved in the pedigree analysis (Fig. 4, B and C). Thus, a transient induction of *NDT80* is sufficient to extend the life span of replicatively aged cells.

To address how transient induction of Ndt80 extends RLS, we monitored age-dependent cellular changes after *NDT80* induction. Neither ERCs nor Hsp104-eGFP aggregates were reduced after *NDT80* induction, although it is possible that they were reduced at later time points (fig. S8, A and B). Furthermore, *NDT80* expression extended life span in the absence of the autophagy gene *ATG1* (fig. S8C). Together these findings suggest that life-span extension can occur in the absence of ERC and Hsp104-aggregate elimination. Although ERCs and Hsp104-eGFP aggregates were not affected by transient *NDT80* expression, nucleolar morphology was. The percentage of aged cells with enlarged nucleolar morphology decreased after *NDT80* induction (Fig. 4, D and E, and fig. S8D). Thus, transient induction of *NDT80* causes a change in nucleolar and/or rDNA structure, which reverts to a state that resembles the morphology of young cells.

We do not yet know whether *NDT80*- and sporulation-induced RLS resetting use the same mechanism(s). The findings that *NDT80* is necessary for life-span extension during sporulation and sufficient for life-span extension during vegetative growth and that nucleolar morphology is altered under both circumstances suggest that at least some processes are shared. Irrespective of the relation between *NDT80*- and sporulation-induced RLS resetting, we note that resetting of RLS provides an opportunity to dissect the molecular causes of aging. For instance, elimination of Hsp104 aggregates and ERCs seem unlikely to be required for *NDT80*-dependent life-span extension, but changes in nucleolar function and/or structure may be important. Intriguingly, rDNA instability and not ERCs per se appear to cause aging in yeast (*23*), and budding yeast cells eliminate most of the nucleolar material during spore packaging (*24*).

It will be interesting to investigate whether our findings extend to other species. In *Caenorhabditis elegans*, a number of longevity mutants exhibit a soma-to-germline transformation that contributes to their enhanced survival (*25*). In mice, reintroduction of telomerase rescues the age-related phenotypes of telomerase-deficient mice (*26*), which suggests that age-dependent cellular damage can be repaired. Our studies suggest that a transient induction of the gametogenesis program in somatic cells removes age-dependent cellular damage and extends life span. Determining how gametogenesis causes the resetting of life span will provide insights into the mechanisms of aging and could facilitate the development of strategies for longevity.

References and Notes

1. A. M. Neiman, *Microbiol. Mol. Biol. Rev.* **69**, 565 (2005).
2. T. Smeal, J. Claus, B. Kennedy, F. Cole, L. Guarente, *Cell* **84**, 633 (1996).
3. M. Boselli, J. Rock, E. Unal, S. S. Levine, A. Amon, *Dev. Cell* **16**, 844 (2009).
4. Materials and methods are available as supporting material on *Science* Online.
5. D. Sinclair, K. Mills, L. Guarente, *Annu. Rev. Microbiol.* **52**, 533 (1998).
6. N. Erjavec, L. Larsson, J. Grantham, T. Nyström, *Genes Dev.* **21**, 2410 (2007).
7. D. A. Sinclair, L. Guarente, *Cell* **91**, 1033 (1997).
8. D. A. Sinclair, K. Mills, L. Guarente, *Science* **277**, 1313 (1997).
9. B. Liu *et al.*, *Cell* **140**, 257 (2010).
10. D. H. Lee, A. L. Goldberg, *J. Biol. Chem.* **271**, 27280 (1996).
11. A.-G. Lenz, H. Holzer, *Arch. Microbiol.* **137**, 104 (1984).
12. T. Kobayashi, T. Horiuchi, *Genes Cells* **1**, 465 (1996).
13. Y. Kassir, D. Granot, G. Simchen, *Cell* **52**, 853 (1988).
14. I. Nachman, A. Regev, S. Ramanathan, *Cell* **131**, 544 (2007).
15. L. Xu, M. Ajimura, R. Padmore, C. Klein, N. Kleckner, *Mol. Cell. Biol.* **15**, 6572 (1995).
16. H. Scherthan *et al.*, *Proc. Natl. Acad. Sci. U.S.A.* **104**, 16934 (2007).
17. S. Klapholz, R. E. Esposito, *Genetics* **96**, 567 (1980).
18. B. H. Lee, A. Amon, *Science* **300**, 482 (2003).
19. S. Chu *et al.*, *Science* **282**, 699 (1998).
20. S. Chu, I. Herskowitz, *Mol. Cell* **1**, 685 (1998).
21. K. R. Benjamin, C. Zhang, K. M. Shokat, I. Herskowitz, *Genes Dev.* **17**, 1524 (2003).
22. T. M. Carlile, A. Amon, *Cell* **133**, 280 (2008).
23. A. R. Ganley, S. Ide, K. Saka, T. Kobayashi, *Mol. Cell* **35**, 683 (2009).
24. J. Fuchs, J. Loidl, *Chromosome Res.* **12**, 427 (2004).
25. S. P. Curran, X. Wu, C. G. Riedel, G. Ruvkun, *Nature* **459**, 1079 (2009).
26. M. Jaskelioff *et al.*, *Nature* **469**, 102 (2011).

Acknowledgments: We thank B. Alpert, M. Boselli, A. Thompson, and J. Chen for technical help; D. Koshland for reagents; and T. Orr-Weaver, F. Solomon, and members of the Amon laboratory for comments on the manuscript. Research was supported by NIH grant GM62207 to A.A. A.A. is also an HHMI investigator. E.Ü. is a fellow of the Jane Coffin Childs Memorial Fund. The authors declare no competing financial interests.

Supporting Online Material

www.sciencemag.org/cgi/content/full/332/6037/1554/DC1
Materials and Methods
SOM Text
Figs. S1 to S8
Table S1
References

15 February 2011; accepted 9 May 2011
10.1126/science.1204349

A Cell Cycle Phosphoproteome of the Yeast Centrosome

Jamie M. Keck,[1]* Michele H. Jones,[1]* Catherine C. L. Wong,[2] Jonathan Binkley,[3] Daici Chen,[4] Sue L. Jaspersen,[5,6] Eric P. Holinger,[1] Tao Xu,[2] Mario Niepel,[7] Michael P. Rout,[8] Jackie Vogel,[4] Arend Sidow,[3] John R. Yates III,[2] Mark Winey[1]†

Centrosomes organize the bipolar mitotic spindle, and centrosomal defects cause chromosome instability. Protein phosphorylation modulates centrosome function, and we provide a comprehensive map of phosphorylation on intact yeast centrosomes (18 proteins). Mass spectrometry was used to identify 297 phosphorylation sites on centrosomes from different cell cycle stages. We observed different modes of phosphoregulation via specific protein kinases, phosphorylation site clustering, and conserved phosphorylated residues. Mutating all eight cyclin-dependent kinase (Cdk)–directed sites within the core component, Spc42, resulted in lethality and reduced centrosomal assembly. Alternatively, mutation of one conserved Cdk site within γ-tubulin (Tub4-S360D) caused mitotic delay and aberrant anaphase spindle elongation. Our work establishes the extent and complexity of this prominent posttranslational modification in centrosome biology and provides specific examples of phosphorylation control in centrosome function.

Phosphorylation is a reversible posttranslational modification that regulates most cellular processes, including the duplication of centrosomes to form the mitotic spindle, which functions in chromosome segregation. Protein kinases, such as cyclin-dependent kinase Cdk1 (Cdc28), Mps1, and Polo kinase (Cdc5) (*1*, *2*), phosphorylate the centrosome, known in yeast as the spindle pole body (SPB; Fig. 1A). The 18 centrosomal proteins (10 have human homologs; Figs. 1B and 2) can be organized into five functional subcomplexes (*1*): the γ-tubulin complex (Tub4, Spc98, and Spc97), which nucleates microtubules; the central core (Nud1, Spc42, Spc29, and Cnm67), which form the organelle's structural foundation and precursor; the linker proteins connecting the core and γ-tubulin complexes; the membrane anchors; and the half-bridge components, where assembly begins. Previous studies examined phosphorylation of these components individually or within whole cell preparations (database S1, column 3). In contrast, we performed

[1]Department of Molecular, Cellular, and Developmental Biology, UCB 347, University of Colorado, Boulder, CO 80309, USA. [2]Department of Chemical Physiology, Scripps Research Institute, La Jolla, CA 92037, USA. [3]Departments of Pathology and Genetics, Stanford University School of Medicine, Stanford, CA 94305, USA. [4]Department of Biology, McGill University, Montreal, Quebec H3G 0B1, Canada. [5]Stowers Institute for Medical Research, Kansas City, MO 64110, USA. [6]Department of Molecular and Integrative Physiology, University of Kansas Medical Center, Kansas City, KS 66160, USA. [7]Department of Systems Biology, Harvard Medical School, Boston, MA 02115, USA. [8]Laboratory of Cellular and Structural Biology, Rockefeller University, 1230 York Avenue, New York, NY 10065, USA.

*These authors contributed equally to this work.
†To whom correspondence should be addressed. E-mail: mark.winey@colorado.edu

a comprehensive analysis of phosphorylation on enriched, intact centrosomes.

Centrosomal complexes were isolated from yeast cells by using a modified affinity purification (*3*) (fig. S1A), and copurifying proteins were analyzed by solution digest and mass spectrometry (MS). Phosphopeptides were enriched with a metal affinity column, processed by liquid chromatography tandem mass spectrometry (LC MS/MS) on an LTQ-Orbitrap mass spectrometer (Thermo Fisher Scientific, San Jose, CA), and identified with SEQUEST and DTASelect2 programs (*4*). DeBunker (*5*) and Ascore (*6*) programs were used to further validate phosphopeptides and phosphorylation assignments, respectively (database S2). Peptides from all 18 proteins were identified, with extensive peptide coverage for most proteins (Fig. 2). The centrosomal preparations (fig. S1B) were highly phosphorylated (fig. S1C), as observed by MS analysis (www.yeastrc.org/pdr/pages/front.jsp; search by protein name). In total, 297 phosphorylation events were mapped on 17 of the 18 yeast centrosomal proteins, of which 227 have not been previously reported.

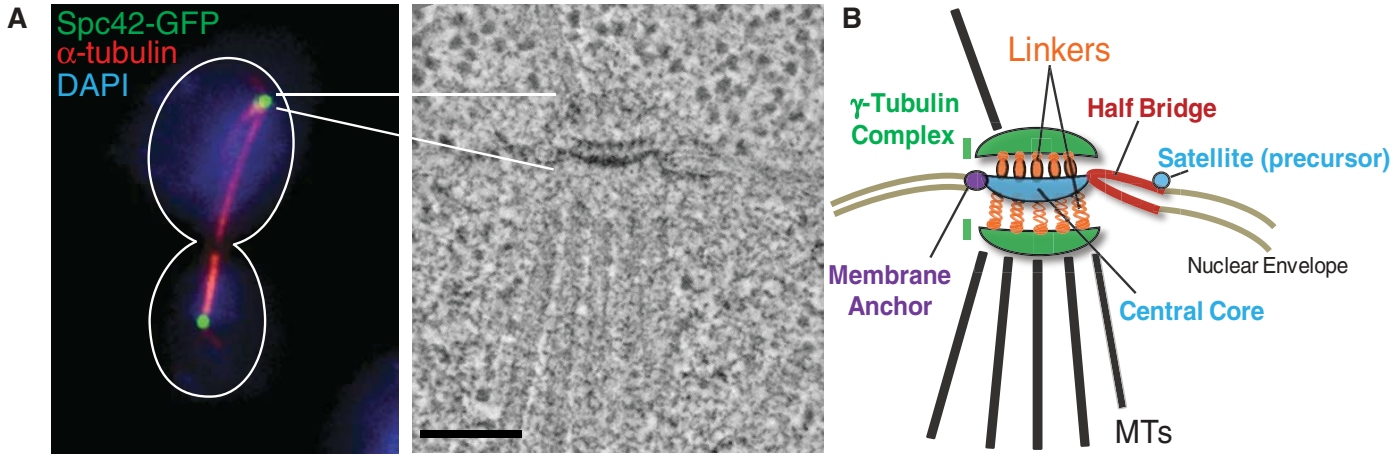

Fig. 1. Yeast centrosomes form the poles of the mitotic spindle and are composed of five subcomplexes. (**A**) Immunofluoresence (left) of a large-budded mitotic yeast cell showing centrosomes marked by Spc42–green fluorescent protein (GFP) (green), microtubules (red), and DNA (blue), and electron micrograph (right) showing trilaminar ultrastructure. Scale bar indicates 100 nm. [Credit: Eileen O'Toole, University of Colorado, Boulder] (**B**) Schematic of the five major functional centrosome subcomplexes. MT indicates microtubule.

Fig. 2. Phosphoproteomic analysis of enriched *Sacchromyces cerevisiae* centrosomes organized by centrosome complexes. Total sites indicates all phosphorylation sites found within all asynchronous, mitotic, and G1 preparations; numbers in parentheses are ambiguous assignments (databases S1 and S2); S/T(P) sites, potential Cdk1 sites; Y sites, tyrosine phosphorylation sites; Coverage, % of the total protein sequence recovered as peptides from mass spectrometry analyses of all centrosome preparations; and human homologs are indicated if applicable. Check marks indicate proteins that are known in vivo or in vitro substrates of Cdk1, Mps1, or Cdc5 kinases (references in fig. S4); dash entries, not observed; asterisks, homologous domains.

Centrosome Proteins	Total Sites	S/T (P) Sites	Y Sites	Coverage	Cdk Kinase	Mps1 Kinase	Cdc5 Kinase	Human Homologs
γ-Tubulin Complex								
Tub4	**8 (1)**	1	2	85%	✓	-	-	**TUBG1**
Spc98	**9**	2	2	65%	✓	✓	-	**TUBGCP3**
Spc97	**5 (1)**	0	1	54%	-	-	-	**TUBGCP2**
Linkers								
Spc110	**31**	3	3	96%	✓	✓	-	**Kendrin**
Spc72	**19 (2)**	3	0	92%	-	-	✓	**TACC***
Cmd1	**7 (1)**	0	0	91%	-	-	-	**Calmodulin**
Core and Satellite								
Nud1	**52 (2)**	5	1	91%	✓	-	✓	**Centriolin**
Spc42	**31 (1)**	6	3	96%	✓	✓	-	
Spc29	**32 (2)**	4	0	100%	✓	✓	-	
Cnm67	**22**	6	3	100%	✓	-	-	
Half Bridge								
Kar1	**7 (1)**	2	0	63%	-	-	-	
Sfi1	**11**	4	0	42%	✓	-	-	**HSfi1**
Cdc31	**4**	0	0	98%	-	✓	-	**Centrin3**
Mps3	**0**	0	0	7%	-	-	-	**SUN domain***
Membrane Anchor								
Nbp1	**27**	6	5	90%	✓	-	-	
Bbp1	**20**	3	2	85%	✓	-	-	
Mps2	**11**	4	0	75%	✓	-	-	
Ndc1	**1**	0	0	24%	-	-	-	
TOTAL:	**297 (11)**	49	22					

Among these are 49 potential Cdk1 sites [S/T-P, serine or threonine followed by proline, 5 are confirmed as Cdk sites (*7*)] and 22 tyrosines (Fig. 2). Combining data from this study (297 sites) and previous studies (29 sites), a total of 326 phosphorylation sites are now identified on the yeast centrosome (database S1).

Because phosphorylation regulates cell cycle events (*8*), including centrosome duplication and mitotic spindle formation, we explored phosphorylation profile differences between centrosomes in cell cycle–arrested cells versus those growing asynchronously. Cells were arrested at an early step of centrosome duplication in late G1 phase with α-factor treatment or in mitosis after centrosome duplication and separation by depletion of the anaphase-promoting complex (APC) activator Cdc20 (fig. S2A). We detected 54 sites that were phosphorylated only in G1, 110 sites that were phosphorylated only in mitosis, and 68 sites phosphorylated in both phases (Fig. 3, fig. S2B, and database S1). The latter 68 sites are likely to be constitutively phosphorylated (because 61 were also found in asynchronous preparations). Of all the subcomplexes, the central core contained the largest number of sites (46% of the total, Fig. 2) and also the highest percentage of all shared sites (72%) (fig. S2C). The 29 mitotic sites on Nud1 may affect its subsequent role in recruitment of cell cycle regulatory proteins required for mitotic exit (*9*). In contrast to the central core, the γ-tubulin complex, linkers, and half-bridge have few constitutive sites and a large number of sites phosphorylated in mitosis.

Analysis of phosphorylated residues that are likely within binding sites or targets of specific kinases showed distinct cell cycle patterns. For example, the majority of sites within Polo (Cdc5) binding motifs (fig. S3A) were observed in mitosis when its activity peaks (*10*). Cell cycle–specific phosphorylation was also observed in 21 of 22 tyrosine sites. In contrast, over half (27 of 49) of the potential Cdk consensus sites were phosphorylated throughout the cell cycle. The constitutive Cdk phosphorylation in Spc42 appeared to be essential, because mutating the Cdk motifs to nonphosphorylatable residues [8 sites out of 32 total phosphorylation sites in Spc42 (fig. S3B)] was lethal. The lethality may result, in part, from the decrease in Spc42 assembly into the centrosome (Fig. 4A). Furthermore, phosphorylation of these Cdk sites is critical for overall Spc42 phosphorylation, because phosphate incorporation decreased in the Spc42-8A mutant by 93% compared with the wild type (WT) (Fig. 4B).

Twelve centrosomal proteins are known substrates of Cdk1 or Mps1 (Fig. 2 and fig. S4A). We performed kinase reactions in vitro with either Cdk1 or Mps1 on our centrosome preparations and identified potential centrosomal substrates by in-gel digestion and MS analysis (fig. S4B). We observed kinase specificity on centrosomal substrates by distinct phosphorylation banding patterns, confirmed several substrates, and identified possible new substrates (Spc72 and Cnm67) for Mps1 and Cdk1, respectively.

Clustering of phosphorylation sites is a rare event that creates a charged region, which can affect protein interactions and contribute to structural integrity (*11*). A study of yeast Cdk phosphorylation showed that a cluster of sites, rather than individual residues, can be evolutionarily conserved (*7*). Clustering was prominent within our centrosomal phosphoproteome, with 174 of the 297 mapped sites clustered in seven proteins [fig. S5, ≥5 sites within 50 residues (*4*)]. Twenty-nine of the 49 Cdk consensus sites were included within these clustered regions. The importance of phosphorylation site clustering is exemplified by analysis of the N terminus of Spc110, which interacts with Spc97 to stabilize the γ-tubulin complex (*12*, *13*). Mutating even 2 out of the 18 phosphorylation sites in this region (fig. S5) is lethal when combined with *spc97* mutations (*14*).

Individual residues that are functionally and structurally important are also conserved through evolution (*15*, *16*). We therefore examined fungal orthologs of centrosomal proteins to determine evolutionary constraint values [measured by positional conservation (*17*, *18*)] for the 297 sites and also regional conservation throughout the proteins [fig. S6; see Fig. 5, A and B, for γ-tubulin (Tub4)]. This analysis identified 59 highly constrained sites in 13 proteins (>80% conserved) and 14 fully conserved residues in 8 proteins (fig. S7, A and B), of which three sites, Tub4-Y445, Spc29-T18, and Spc29-T240 (*19*), are essential for centrosome function (*20*–*22*). Fourteen sites from this study are conserved in human centrosomal proteins (fig. S7C).

The phosphorylated residue, S360 (*19*), within γ-tubulin (Tub4) (fig. S8A) is fully conserved in fungi (Fig. 5B and fig. S6) and in humans (fig. S8B). γ-Tubulin is part of an evolutionarily conserved complex (γ-tubulin small complex, γ-tuSC) that nucleates microtubules for chromosome segregation. Phosphorylation of γ-tubulin has been shown to promote centrosome duplication and microtubule assembly (*20*, *23*). Tub4-S360 lies within a Cdk motif and is phosphorylated by Cdk1 in vitro (fig. S8, C and D). This site is located within a surface loop available for protein-protein interactions, as viewed in the γ-tubulin crystal structure (Fig. 5C, star). Furthermore, structural analysis using cryo-electron microscopy

Centrosome Proteins	Total Asynch	Unique Asynch	Total G1	Unique G1	Total Mitotic	Unique Mitotic	Shared G1/M
γ-TubulinComplex							
Tub4	0	0	2	2	6	6	0
Spc98	3	3	3	2	4	3	1
Spc97	0	0	3	3	2	2	0
Linkers							
Spc110	16	6	14	9	16	11	5
Spc72	5	2	2	2	15	15	0
Cmd1	4	4	1	1	2	2	0
Core and Satellite							
Nud1	27	10	13	2	40	29	11
Spc42	25	1	20	3	27	10	17
Spc29	26	8	18	8	16	6	10
Cnm67	16	2	15	4	16	5	11
Half Bridge							
Kar1	6	3	0	0	4	4	0
Sfi1	7	4	2	2	5	5	0
Cdc31	3	2	1	0	2	1	1
Mps3	0	0	0	0	0	0	0
Membrane Anchor							
Nbp1	20	10	12	7	10	5	5
Bbp1	12	4	12	6	10	4	6
Mps2	9	6	4	3	2	1	1
Ndc1	1	0	0	0	1	1	0
TOTAL:	180	**65**	122	**54**	178	**110**	**68**

Fig. 3. *S. cerevisiae* centrosome phosphorylation is dynamic during the cell cycle and is enriched in mitosis. Total Asynch, all sites found in asynchronous preparations or Unique, only in Asynch; Total G1, all sites found in G1 preparations or Unique in G1 (not in mitotic preparations); Total Mitotic, all sites found in mitotic preparations or Unique in mitotic (not in G1 preparations); Shared G1/M, sites found in mitotic and G1 preparations.

of the yeast γ-tubulin complex places this loop directly between Spc98 and Spc97 (*13*). Therefore, we mutated S360 to either a nonphosphorylatable alanine (A) or an aspartic/glutamic acid (D or E) to mimic constitutive phosphorylation. The *tub4-S360A* allele did not affect growth; however, *tub4-S360D* and *tub4-S360E* caused growth defects at 25°C and mitotic arrest resulting in cell death upon shift to a higher temperature (37°C) (fig. S9, A to C). Also, *tub4-S360D* was lethal in combination with mutations in *SPC98* (*spc98-2*), by deletion of the spindle checkpoint gene *MAD2*

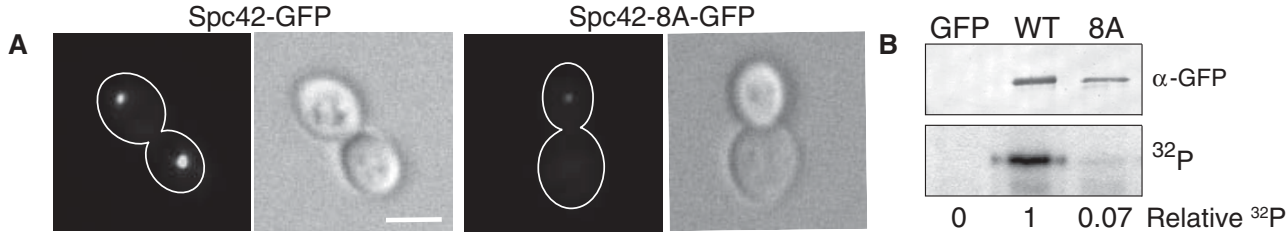

Fig. 4. Effect of mutating all Cdk sites within the core protein, Spc42. (**A**) Incorporation of Spc42-GFP and Spc42-8A-GFP into the two centrosomes, analyzed by fluorescence microscopy (n = 200). Phase microscopy images show large-budded mitotic cells. Scale bar, 5 μm. (**B**) Relative ^{32}P incorporation into GFP, Spc42-GFP (WT), and Spc42-8A-GFP (8A) proteins upon protein induction in yeast cells shown by anti-GFP Western blot (top) and autoradiograph (bottom). Quantified by phosphorimager (below) and normalized to α-GFP signal, n = 3.

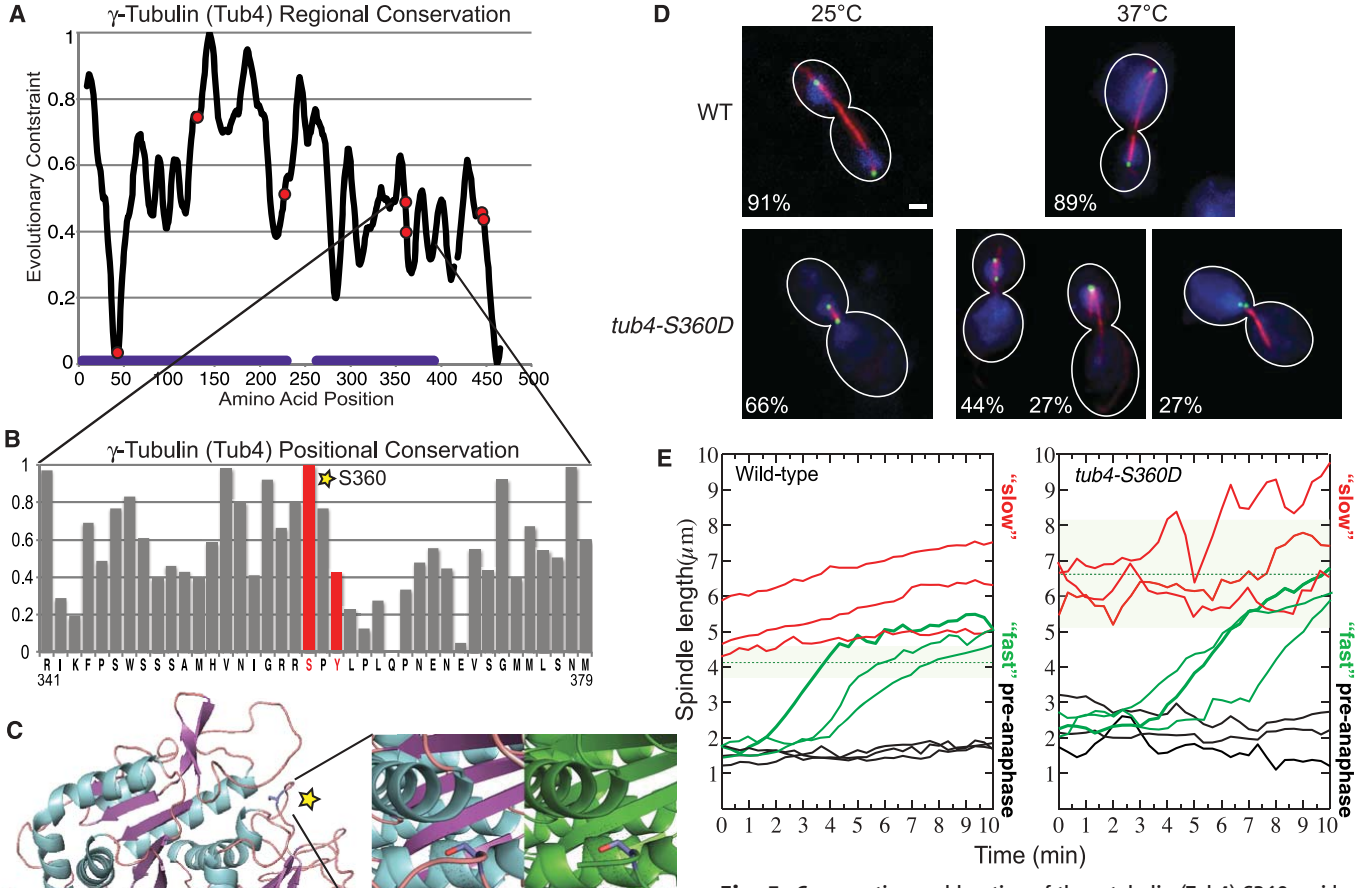

Fig. 5. Conservation and location of the γ-tubulin (Tub4) S360 residue and phenotype of the phosphomimetic, *Tub4-S360D*. (**A**) γ-Tubulin (Tub4) regional evolutionary constraint among fungi (20 amino acid sliding regions). Red dots represent phosphorylation sites identified in this study. *Y* axis, constraint; a value of 1 is fully conserved. *X* axis, amino acid position; purple lines, P-Fam domains (GTP binding and C-terminal domains). (**B**) Positional constraint histogram for amino acids 341 to 379 (*19*) within γ-tubulin (Tub4). Red columns are phosphorylated residues; star marks S360. *Y* axis, constraint; 1 is fully conserved. *X* axis, protein sequence. (**C**) Comparative model of yeast Tub4, generated by PyMOL (www.pymol.org), threaded onto the x-ray crystallographic structure of human γ-tubulin (*4*). Star marks position of Tub4-S360 in an exposed loop, expanded in inset and compared with human S364. (**D**) Immunofluorescence of mitotic spindles from WT and *tub4-S360D* cells at 25°C and 37°C. Centrosomes (Spc42-GFP, green), microtubules (anti–α-tubulin, red), and DNA [4′,6′-diamidino-2-phenylindole (DAPI), blue] are shown. % indicates the percentage of cells with shown spindle structure, n = 200 cells for each. Scale bar, 1.5 μm. (**E**) Live cell analysis of spindle length for WT and *tub4-S360D* cells at 25°C. Centrosomes labeled by Spc42-CFP (cyan fluorescent protein). Each time step is 20 s. Spindle length (μm) measured by mother and daughter pole displacement (*4*). Spindle lengths are shown in black (metaphase), green (fast anaphase), and red (slow anaphase) and are representative for WT (n = 17) and *tub4-S360D* (n = 18) strains. Green hashed line is mean transition length, and green shaded shows standard deviation.

(*mad2*Δ) that allows for correction of mitotic defects, and by deletion of the EB1 homolog *BIM1* (*bim1*Δ), which is involved in microtubule dynamics (fig. S9A).

These genetic interactions suggested that *tub4-S360D* cells had defects in mitotic spindle assembly, which we analyzed by immunofluorescence microscopy and live cell imaging. At 25°C the majority (66%) of spindles in *tub4-S360D* large-budded mitotic cells had not extended past metaphase length [~1.5 μm (*24*)], whereas WT cells (91%) had normal elongated anaphase spindles [6 to 10 μm (*24*)] (Fig. 5D, 25°C). This phenotype was exacerbated at 37°C, with 98% of *tub4-S360D* cells containing either adjacent or unresolvable spindle poles (54%) or metaphase-length spindles (44%) (Fig. 5D), compared with WT cells (89% normal anaphase spindles). Live cell analysis of microtubules in *tub4-S360D* cells grown at 25°C revealed that spindles persisted longer in the fast phase (*25*) of anaphase spindle elongation (Fig. 5E, green lines), resulting in a transition to the slow phase (*25*) with longer anaphase spindles [6.6 μm ± 1.5 (SEM)] than WT cells [4.1 μm ± 0.4 (SEM); $P < 0.001$] (Fig. 5E, dashed green lines). In addition, large spindle length fluctuations were observed in *tub4-S360D* cells before anaphase (Fig. 5E, black lines; quantified in fig. S10) and in the slow phase of anaphase (Fig. 5E, red lines). Thus, phosphorylation of a single Cdk site in γ-tubulin appears to contribute to proper dynamics of anaphase spindle microtubules.

Phosphoregulation of the centrosome is likely to be conserved, not only with respect to the protein kinases but also through specific residues in the respective human homologs. Illustrated by our analysis of γ-tubulin and Spc42, the conserved residues and phosphorylation patterns in yeast will be useful tools for studying the human centrosome, a much larger (>100 proteins) and more complicated microtubule organizing center.

References and Notes

1. S. L. Jaspersen, M. Winey, *Annu. Rev. Cell Dev. Biol.* **20**, 1 (2004).
2. K. Crasta, H. H. Lim, T. H. Giddings Jr., M. Winey, U. Surana, *Nat. Cell Biol.* **10**, 665 (2008).
3. M. Niepel, C. Strambio-de-Castillia, J. Fasolo, B. T. Chait, M. P. Rout, *J. Cell Biol.* **170**, 225 (2005).
4. Materials and methods are available as supporting material on *Science* Online.
5. B. Lu, C. Ruse, T. Xu, S. K. Park, J. Yates 3rd, *Anal. Chem.* **79**, 1301 (2007).
6. S. A. Beausoleil, J. Villén, S. A. Gerber, J. Rush, S. P. Gygi, *Nat. Biotechnol.* **24**, 1285 (2006).
7. L. J. Holt *et al.*, *Science* **325**, 1682 (2009).
8. D. O. Morgan, *Nature* **374**, 131 (1995).
9. R. Visintin, A. Amon, *Mol. Biol. Cell* **12**, 2961 (2001).
10. J. L. Snead *et al.*, *Chem. Biol.* **14**, 1261 (2007).
11. R. Schweiger, M. Linial, *Biol. Direct* **5**, 6 (2010).
12. D. B. Vinh, J. W. Kern, W. O. Hancock, J. Howard, T. N. Davis, *Mol. Biol. Cell* **13**, 1144 (2002).
13. J. M. Kollman, J. K. Polka, A. Zelter, T. N. Davis, D. A. Agard, *Nature* **466**, 879 (2010).
14. D. B. Friedman *et al.*, *J. Biol. Chem.* **276**, 17958 (2001).
15. M. Kimura, *The Neutral Theory of Molecular Evolution* (Cambridge Univ. Press, Cambridge, 1983).
16. A. N. Ba, A. M. Moses, *Mol. Biol. Evol.* **27**, 2027 (2010).
17. I. Mayrose, D. Graur, N. Ben-Tal, T. Pupko, *Mol. Biol. Evol.* **21**, 1781 (2004).
18. J. Binkley *et al.*, *Genome Res.* **20**, 142 (2010).
19. Single-letter abbreviations for the amino acid residues are as follows: A, Ala; C, Cys; D, Asp; E, Glu; F, Phe; G, Gly; H, His; I, Ile; K, Lys; L, Leu; M, Met; N, Asn; P, Pro; Q, Gln; R, Arg; S, Ser; T, Thr; V, Val; W, Trp; and Y, Tyr.
20. J. Vogel *et al.*, *Dev. Cell* **1**, 621 (2001).
21. Y. Araki *et al.*, *J. Cell Biol.* **189**, 41 (2010).
22. E. P. Holinger *et al.*, *J. Biol. Chem.* **284**, 12949 (2009).
23. M. Alvarado-Kristensson, M. J. Rodríguez, V. Silió, J. M. Valpuesta, A. C. Carrera, *Nat. Cell Biol.* **11**, 1081 (2009).
24. M. Winey, E. T. O'Toole, *Nat. Cell Biol.* **3**, E23 (2001).
25. J. A. Kahana, B. J. Schnapp, P. A. Silver, *Proc. Natl. Acad. Sci. U.S.A.* **92**, 9707 (1995).

Acknowledgments: We thank C. Pearson, A. Stemm-Wolf, and T. Su for comments on the manuscript; T. Davis and the Winey lab for helpful discussions; E. O'Toole for the electron micrograph; E. Nazarova for assisting with spindle dynamics analysis; M. Riffle for Yeast Resource Center assistance; and D. D'amours for the Cdc28 purification protocol. This work was supported by NIH U54 RR022220 and R01 GM062427 (M.P.R.), NIH R01 HG003039 (A.S.), NIH P41 RR011823 (J.R.Y. III, T.N. Davis, principal investigator), CIHR MOP-64404 (J.V.), and NIH GM51312 (M.W.). J.M.K. was supported by NIH F32 GM086038, and E.P.H. was supported by NIH T32 GM008759. Mass spectrometry data are provided at the Yeast Resource Center (www.yeastrc.org/pdr/pages/front.jsp).

Supporting Online Material

www.sciencemag.org/cgi/content/full/332/6037/1557/DC1
Materials and Methods
Figs. S1 to S10
Table S1
References
Databases S1 and S2

7 March 2011; accepted 17 May 2011
10.1126/science.1205193

Mutagenic Processing of Ribonucleotides in DNA by Yeast Topoisomerase I

Nayun Kim,[1] Shar-yin N. Huang,[2] Jessica S. Williams,[3] Yue C. Li,[1] Alan B. Clark,[3] Jang-Eun Cho,[1] Thomas A. Kunkel,[3] Yves Pommier,[2] Sue Jinks-Robertson[1]*

The ribonuclease (RNase) H class of enzymes degrades the RNA component of RNA:DNA hybrids and is important in nucleic acid metabolism. RNase H2 is specialized to remove single ribonucleotides [ribonucleoside monophosphates (rNMPs)] from duplex DNA, and its absence in budding yeast has been associated with the accumulation of deletions within short tandem repeats. Here, we demonstrate that rNMP-associated deletion formation requires the activity of Top1, a topoisomerase that relaxes supercoils by reversibly nicking duplex DNA. The reported studies extend the role of Top1 to include the processing of rNMPs in genomic DNA into irreversible single-strand breaks, an activity that can have distinct mutagenic consequences and may be relevant to human disease.

The exclusion and removal of single ribonucleotides [ribonucleoside monophosphates (rNMPs)] from DNA are important for the stability and function of the genome. In *Saccharomyces cerevisiae*, the introduction of an rNMP-permissive form of DNA polymerase ε into a strain lacking ribonuclease (RNase) H2 confers a mutator phenotype and is associated with the accumulation of a distinct mutation class: deletions within short [2– to 5–base pairs (bp)] tandem repeats (*1*). In contrast to similar mutations initiated by DNA polymerase slippage during genome replication, however, the rNMP-associated deletion intermediates are not substrates for the postreplicative mismatch repair machinery (*2*). A similar deletion signature is associated with high levels of transcription in yeast and requires the activity of Top1 (*3*, *4*), a type 1B topoisomerase important for removing transcription-associated supercoils (*5*). Here, we demonstrate that rNMP-associated deletions are likewise dependent on Top1 activity, map in vitro the positions of Top1 cleavage at deletion hotspots identified in vivo, and confirm that Top1 has endoribonuclease activity when an rNMP is substituted at the scissile phosphate.

The *CAN1* gene encodes arginine permease, the loss of which confers resistance to the toxic arginine analog canavanine (Can-R phenotype). To determine the effect of persistent rNMPs on *CAN1* mutagenesis in yeast, we deleted the *RNH201* gene, which encodes the catalytic subunit of RNase H2 (*6*, *7*). Though there was only a small elevation in the Can-R rate in the *rnh201* background, there was a substantial change in the corresponding mutation spectrum, with ~40% of mutations

[1]Department of Molecular Genetics and Microbiology, Duke University Medical Center, Durham, NC 27710, USA. [2]Laboratory of Molecular Pharmacology, Center for Cancer Research, National Cancer Institute, National Institutes of Health, Bethesda, MD 20892, USA. [3]Laboratory of Molecular Genetics and Laboratory of Structural Biology, National Institute of Environmental Health Sciences, National Institutes of Health, Research Triangle Park, NC 27709, USA.

*To whom correspondence should be addressed. E-mail: sue.robertson@duke.edu